High Frequency Images of Proud and Buried 3D-Targets

Gary Steven Sammelmann, Coastal Systems Station
Code R21
6703 West Highway 98
Panama City, Florida 32407-3560
SammelmannGS@NCSC.Navy.Mil

Abstract
PC SWAT (Personal Computer Shallow Water Acoustic Tool-set) is a sonar simulation package developed at Coastal Systems Station to predict acoustic sensor performance. This article focuses on the algorithms used by PC SWAT to generate synthetic images of proud, buried, and partially buried three-dimensional targets. High frequency scattering from the target is described by a combination of the Kirchhoff approximation and the Geometric Theory of Diffraction. Propagation of sound into a marine sediment with ripples is described by an application of Snell's law and second order perturbation theory in terms of Bragg scattering.

I. INTRODUCTION

This article focuses on the techniques used by version 8.0 of PC SWAT (Personal Computer Shallow Water Acoustic Tool-set) to create synthetic images of buried and partially buried 3-dimensional targets in the presence of sand ripples. PC SWAT computes the incoming and outgoing eigen-rays to reference point in the vicinity of the buried target. Based upon the grazing angle of the incoming and outgoing eigen-rays at the target, PC SWAT uses the second order perturbation theory of Moe[1] to describe Snell's law and Bragg scattering of sound into and from a sediment with sand ripples. PC SWAT then combines the eigen-rays in the water column and the sediment to obtain the eigen-rays to and from individual facets and edges on the target. Scattering from facets are described by the Kirchhoff approximation[2].

Section II outlines the model for constructing the eigen-rays into and from the sediment based on the second order perturbation theory described by Moe[1]. Section III contains sample calculations of buried and partially buried targets showing the effects of sand ripples on images of 3D targets. Finally, section IV concludes.

II. SEDIMENT PENETRATION

The following section describes the model for scattering from and out of the bottom with sand ripples. This work is based on the second order perturbation theory[1] of scattering from sand ripples. It assumes that the scattering into the sediment is approximately described by Snell's law for angles above the critical angle, and by second order perturbation theory below the critical angle. This section ignores the effects of small-scale roughness and volume inhomogeneities.

Let ϑ_i be the grazing angle of the incident field, and φ be the azimuthal angle between the incident field and the direction of the ripple field. Neglecting small-scale roughness, the scattering into the sediment is composed of five terms. The first is the coherent component due to Snell's law. The remaining components are the lowest order terms for Bragg diffraction of sound into the sediment by the ripple structure. It is these last remaining terms that play the dominant role of scattering into the sediment for sub-critical grazing angles.

This section assumes the sinusoidal surface is of the following form.

$$z = h_R \cos(k_R x) \tag{2.1}$$

The incident wave vector is of the following form, where we assume the ripples are oriented along the x-axis.

$$\begin{aligned} k_{i,x} &= k_1 \cos(\vartheta_i)\cos(\varphi) \\ k_{i,y} &= k_1 \cos(\vartheta_i)\sin(\varphi) \\ k_{i,z} &= k_1 \sin(\vartheta_i) \end{aligned} \tag{2.2}$$

Here, k_1 and k_2 are the angular wavenumber in the fluid and the sediment, respectively.

Report Documentation Page

Form Approved
OMB No. 0704-0188

1. REPORT DATE	2. REPORT TYPE	3. DATES COVERED
01 SEP 2003	**N/A**	**-**

4. TITLE AND SUBTITLE	5a. CONTRACT NUMBER
High Frequency Images of Proud and Buried 3D-Targets	5b. GRANT NUMBER
	5c. PROGRAM ELEMENT NUMBER
6. AUTHOR(S)	5d. PROJECT NUMBER
	5e. TASK NUMBER
	5f. WORK UNIT NUMBER
7. PERFORMING ORGANIZATION NAME(S) AND ADDRESS(ES) **Coastal Systems Station Code R21 6703 West Highway 98 Panama City, Florida 32407-3560**	8. PERFORMING ORGANIZATION REPORT NUMBER
9. SPONSORING/MONITORING AGENCY NAME(S) AND ADDRESS(ES)	10. SPONSOR/MONITOR'S ACRONYM(S)
	11. SPONSOR/MONITOR'S REPORT NUMBER(S)

12. DISTRIBUTION/AVAILABILITY STATEMENT
Approved for public release, distribution unlimited

13. SUPPLEMENTARY NOTES
See also ADM002146. Oceans 2003 MTS/IEEE Conference. Held in San Diego, California on September 22-26, 2003. U.S. Government or Federal Purpose Rights License, The original document contains color images.

14. ABSTRACT

15. SUBJECT TERMS

16. SECURITY CLASSIFICATION OF:			17. LIMITATION OF ABSTRACT	18. NUMBER OF PAGES	19a. NAME OF RESPONSIBLE PERSON
a. REPORT	b. ABSTRACT	c. THIS PAGE			
unclassified	**unclassified**	**unclassified**	**UU**	**7**	

The horizontal wavenumber of the incident field is of the following form.

$$q_{i,x} = k_1 \cos(\vartheta_i)\cos(\varphi)$$
$$q_{i,y} = k_1 \cos(\vartheta_i)\sin(\varphi) \tag{2.3}$$

The vertical wavenumber in the upper and lower media are given by the following functions of the horizontal wavenumber, where the branch cut is chosen such that the imaginary component of the wavenumber on the physical sheet is positive.

$$h_1(\vec{q}) = i\sqrt{q^2 - k_1^2}$$
$$h_2(\vec{q}) = i\sqrt{q^2 - k_2^2} \tag{2.4}$$

The plane wave reflection coefficient is given by the following expression in terms of the vertical wavenumber and the ratio of the density of the sediment to that of seawater.

$$R(\vec{q}) = (\rho h_1(\vec{q}) - h_2(\vec{q}))/(\rho h_1(\vec{q}) + h_2(\vec{q})) \tag{2.5}$$

The following vector gives the horizontal wavenumber of the ripple field.

$$q_{R,x} = k_R \equiv 2\pi / L_R$$
$$q_{R,y} = 0 \tag{2.6}$$

To second order in perturbation theory, Bragg scattering through a sinusoidal surface consists of 5 rays whose horizontal wavenumber are of the following form, where n ranges from –2 to +2.

$$\vec{q}_f = \vec{q}_i + n\vec{k}_R \tag{2.7}$$

Define the following quantities taken from Moe[1].

$$a = 1 - \frac{k_2^2}{\rho k_1^2} + (\frac{1}{\rho} - 1)\frac{\vec{q}_f \bullet \vec{q}_i}{k_1^2}$$
$$b = (\rho - 1)\frac{h_1(\vec{q}_f)h_1(\vec{q}_i)}{k_1^2} \tag{2.8}$$

$$H_{11}(\vec{q}_f, \vec{q}_i) = \frac{k_1}{2ih_1(\vec{q}_f)}\{a(1 + R(\vec{q}_f))(1 + R(\vec{q}_i))$$
$$+b(1 - R(\vec{q}_f))(1 - R(\vec{q}_i))\} \tag{2.9}$$

$$H_{12}(\vec{q}_f, \vec{q}_i) = \frac{k_1}{2ih_1(\vec{q}_f)}\{a(1 + R(\vec{q}_f))(1 + R(\vec{q}_i))$$
$$-b(1 + R(\vec{q}_f))(1 - R(\vec{q}_i))\} \tag{2.10}$$

$$G_{11}(\vec{q}_f, \vec{q}\,', \vec{q}_i) =$$
$$\frac{1}{2}(\frac{k_2^2}{k_1^2} - 1)\{(1 + R(\vec{q}_f))(1 - R(\vec{q}_i))\frac{h_1(\vec{q}_i)}{h_1(\vec{q}_f)}$$
$$-(1 - R(\vec{q}_f))(1 + R(\vec{q}_i))\}$$
$$+\frac{ik_1 H_{11}(\vec{q}\,', \vec{q}_i)}{h_1(\vec{q}_f)}\{(\frac{\vec{q}_f \bullet \vec{q}\,'}{k_1^2} - 1)(1 + R(\vec{q}_f))$$
$$-\frac{h_1(\vec{q}_f)h_1(\vec{q}\,')}{k_1^2}(1 - R(\vec{q}_f))\}$$
$$+\frac{ik_1 H_{12}(\vec{q}\,', \vec{q}_i)}{h_1(\vec{q}_f)}(1 + R(\vec{q}_f))\{\frac{k_2^2 - \vec{q}_f \bullet \vec{q}\,'}{\rho k_1^2}$$
$$-\frac{\rho h_1(\vec{q}_f)h_1(\vec{q}\,')}{k_1^2}\frac{(1 - R(\vec{q}_f))}{(1 + R(\vec{q}_f))}\frac{(1 - R(\vec{q}\,'))}{(1 + R(\vec{q}\,'))}\} \tag{2.11}$$

$$G_{12}(\vec{q}_f, \vec{q}\,', \vec{q}_i) = G_{11}(\vec{q}_f, \vec{q}\,', \vec{q}_i)$$
$$-\frac{h_1(\vec{q}_i)h_1(\vec{q}_i)}{k_1^2}(1 + R(\vec{q}_i)) + \frac{h_2(\vec{q}_i)h_2(\vec{q}_i)}{k_1^2}(1 + R(\vec{q}_i))$$
$$+\frac{2ik_1 H_{11}(\vec{q}\,', \vec{q}_i)}{h_1(\vec{q}\,')} + \frac{2ih_2(\vec{q}\,')H_{12}(\vec{q}\,', \vec{q}_i)}{k_1} \tag{2.13}$$

The T-matrix for the 5 Bragg waves diffracted into the sediment is given by the following expressions.

$$T_{12}(\vec{q}_i, \vec{q}_i) =$$
$$(1 + R(\vec{q}_i)) + \frac{1}{2}(\frac{k_1 h_R}{2})^2\{G_{12}(\vec{q}_i, \vec{q}_i - \vec{q}_R, \vec{q}_i) + G_{12}(\vec{q}_i, \vec{q}_i + \vec{q}_R, \vec{q}_i)\}$$
$$T_{12}(\vec{q}_i - \vec{q}_R, \vec{q}_i) = \frac{k_1 h_R}{2}H_{12}(\vec{q}_i - \vec{q}_R, \vec{q}_i)$$
$$T_{12}(\vec{q}_i + \vec{q}_R, \vec{q}_i) = \frac{k_1 h_R}{2}H_{12}(\vec{q}_i + \vec{q}_R, \vec{q}_i)$$
$$T_{12}(\vec{q}_i + 2\vec{q}_R, \vec{q}_i) = \frac{1}{2}(\frac{k_1 h_R}{2})^2 G_{12}(\vec{q}_i + 2\vec{q}_R, \vec{q}_i + \vec{q}_R, \vec{q}_i)$$
$$T_{12}(\vec{q}_i - 2\vec{q}_R, \vec{q}_i) = \frac{1}{2}(\frac{k_1 h_R}{2})^2 G_{12}(\vec{q}_i - 2\vec{q}_R, \vec{q}_i - \vec{q}_R, \vec{q}_i) \tag{2.14}$$

Reciprocity yields the following expression for the outgoing T-matrix in terms of the incoming T-matrix[3-4].

$$T_{21}(-\vec{q}_i,-\vec{q}_f)=\frac{h_2(\vec{q}_f)}{\rho h_1(\vec{q}_i)}T_{12}(\vec{q}_f,\vec{q}_i) \qquad (2.15)$$

The pressure field of the Bragg waves scattered into the sediment is given by the following expression in terms of the incoming T-matrix, where z is the depth into the sediment.

$$p=T_{12}(\vec{q}_i+n\vec{q}_R,\vec{q}_i)\exp[+ih_2(\vec{q}_i+n\vec{q}_R)z] \qquad (2.16)$$

Similarly, the pressure field scattered from the sediment into the water column is given by the following expression.

$$p=T_{21}(-\vec{q}_i,-(\vec{q}_i+n\vec{q}_R))\exp[+ih_2(\vec{q}_i+n\vec{q}_R)z]$$
$$=\frac{h_2(\vec{q}_i+n\vec{q}_R)}{\rho h_1(\vec{q}_i)}T_{12}(\vec{q}_i+n\vec{q}_R,\vec{q}_i)\exp[+ih_2(\vec{q}_i+n\vec{q}_R)z] \qquad (2.17)$$

The travel time of the individual paths are estimated from the vertical wavenumber in the sediment by the following expression.

$$t=\frac{\mathrm{Re}(k_2)}{\mathrm{Re}(h_2)}\frac{z}{c_2} \qquad (2.18)$$

Here c_2 is the speed of sound in the sediment and z is the burial depth.

III SAMPLE CALCULATIONS

This section contains sample calculations of the images of buried and partially buried 3D targets. This section uses the combination of the Kirchhoff approximation and Geometric Theory of Diffraction described by Sammelmann[2] to compute the scattered field given the incoming and outgoing eigen-rays.

Figure 1 depicts the image of a buried cylinder at broad side incidence taken by the Low Frequency Synthetic Aperture Sonar (LFSAS) during SAX99[5]. The center frequency of the sonar is 20 kilohertz with a bandwidth of 10 kilohertz. The elements are 15 cm in length with a vertical beam width of 25 degrees. The sonar is a synthetic aperture sonar with a resolution of 7.5cm x 7.5cm. The cylinder is buried approximately 35cm from the center of the cylinder. The cylinder is 2 meters in length and 0.50 meters in diameter. The target is located at a range of 25 meters from the sonar, which is operating at an altitude of 4 meters. The incident grazing angle at the target is approximately 10 degrees, which is well below the critical grazing angle of medium sand. The measured signal-to-noise ratio of the target is approximately 20 decibels.

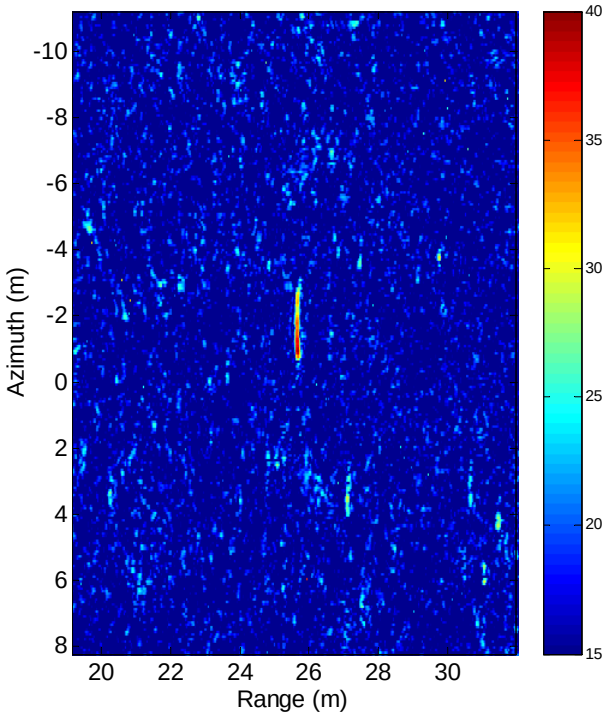

Figure 1. SAX99 image of buried cylinder.

Figure 2 depicts a synthetic image of a similar target buried 36 cm at a range of 20 meters for the LFSAS as computed by PC SWAT 8.0 using the methods outlined in the previous section. The altitude of the sonar is 4 meters with a depression angle of 5 degrees. The center frequency of the sonar is 20 kilohertz with a bandwidth of 10 kilohertz. Both the projector and receiver are 15 cm in length with a vertical beam-width of 25 degrees. The ripple height is 2 cm with a ripple wavelength of 25 cm as opposed to the 75 cm wavelength reported for SAX99. In the case the ripple wavelength is 75 cm, the target is not discernible above the background. The shorter ripple wavelength produces a more vertically oriented Bragg diffracted wave. Qualitatively the two images are similar, but the signal-to-noise ratios between the two cases are greatly different. The signal-to-noise ratio in Figure 2 is approximately 15 decibels. Sediment penetration is largely due to Bragg scattering. The difference between the two images is likely due to the fact that higher order Bragg scattering terms are responsible for the signal in Figure 1, resulting in a propagation path that is

more vertical than that predicted by the second order Bragg scattering term.

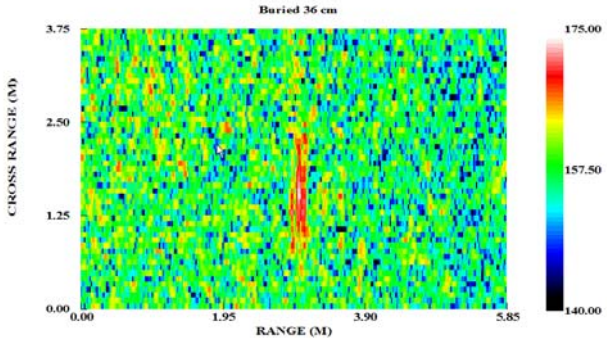

Figure 2. PCSWAT image of buried cylinder.

When the wavelength of the ripple is much greater than that of the incident field the effect of higher order terms in perturbation theory is to introduce terms with a horizontal wave number of the following form.

$$k_x = k_{i,x} - nk_R$$
$$k_y = k_{i,y} \qquad (3.1)$$

Here, *n* is an integer. In the case $k_R << k_{i,x}$, increasing the integer n results in a smaller horizontal wave number corresponding to a wave that is more nearly vertically directed. This trend continues up to a critical value for n, beyond which the wave begins to propagate in the backward direction and becomes more nearly horizontal. Those higher order terms that are more vertically oriented, travel less distance in the sediment and are less affected by the attenuation in the sediment. In the case of first order perturbation theory, Bragg scattering consists of the terms $n = -1, +1$. In the case of second order perturbation theory, Bragg scattering consists of the terms $n = -2, 0, +2$.

Figure 3 depicts a plot of the two-way transmission loss for a medium sand bottom at a frequency of 20 kilohertz in the presence of sand ripples in the case the incident field is oriented at 0, 45, and 90 degrees relative to the sand ripples. The wave height of the ripple is 2 cm and the wavelength is 75 cm. Bragg scattering from the ripples significantly increases sediment penetration past the critical angle at broadside incidence (0 degrees). Sediment penetration below the critical angle for an incident field parallel to the ripple field (90 degrees) is due to the evanescent field and the random, small-scale roughness of the surface.

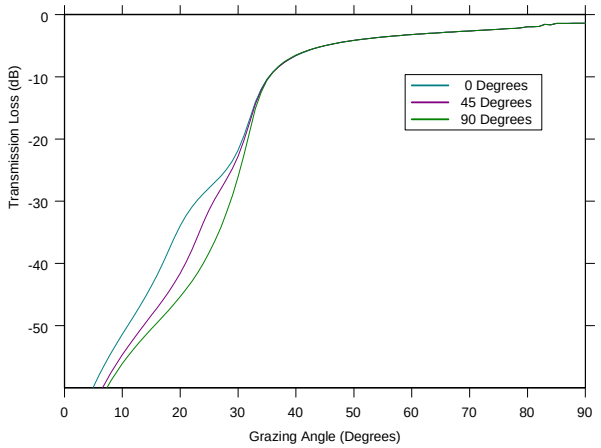

Figure 3. Transmission loss versus orientation relative to the ripple field.

Figure 4 depicts a comparison of two-way transmission loss as a function of grazing angle for first and second order perturbation theory at 20 kilohertz for a target buried 10 cm. The ripple height is 2 cm and the ripple wavelength is 25 cm. Decreasing the ripple wavelength has significantly increased the sediment penetration at low grazing angles.

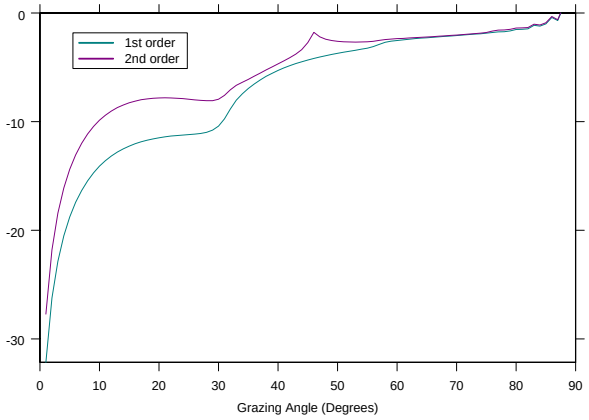

Figure 4. Comparison of two-way transmission loss

Figure 5 depicts an image of a partially buried 81 mm mortar shell at the top of the image, a buried sphere 8 inches in diameter in the middle of the image, and a partially buried 100 mm artillery shell at the bottom of the image. The center frequency of the sonar is 45 kilohertz with a band-width of 20 kilohertz. Both the projector and receiver are conical elements with a diameter of 8 cm. The altitude of the sonar is 2 m with a depression angle of 25 degrees. The sonar is operated in SAS mode, where the distance between successive pings is 2.5 cm. The targets are approximately 2.5 to 3.5 meters from the sonar. Both the mortar and artillery shell are near broad side incidence. In the case of the mortar shell, the fins of the mortar shell are in evidence in

the image. The image is plotted on a 50 decibels logarithmic scale, where the units on the axes are meters.

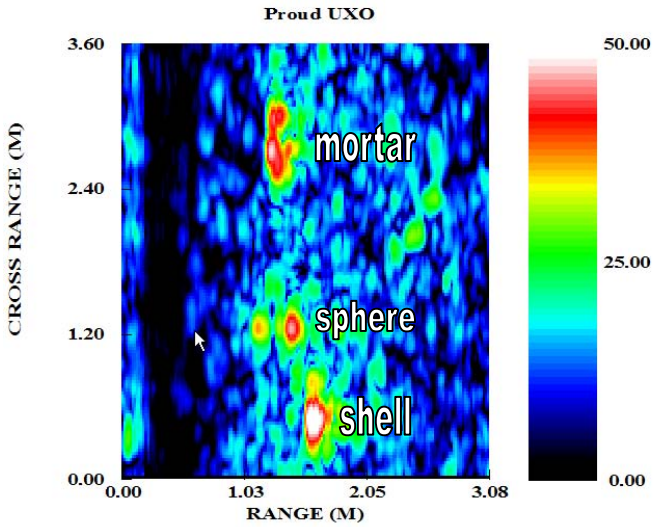

Figure 5. Image of partially buried and buried UXO.

Figure 6 depicts a simulated image of a partially buried 81 mm mortar shell and 100 mm artillery shell computed by PC SWAT 8.0. The image is plotted on a 50 decibels logarithmic scale. The axes are labeled in meters. Figure 7 depicts a blow up of the image of the area around the mortar shell. The head and fins of the mortar shell are in evidence in the simulated image. Figure 8 depicts a blown up image of the area around the 100 mm artillery shell. Figure 9 depicts an outline of the shape of the mortar shell used in PC SWAT. Figure 10 depicts an outline of the 100 mm artillery shell used in PC SWAT.

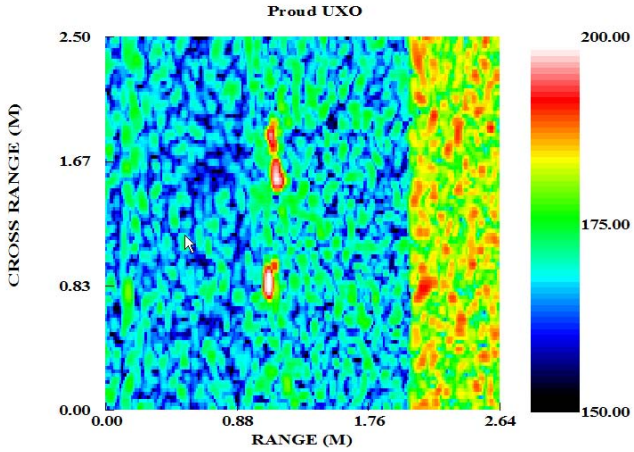

Figure 6. Simulated image of partially buried mortar and artillery shell.

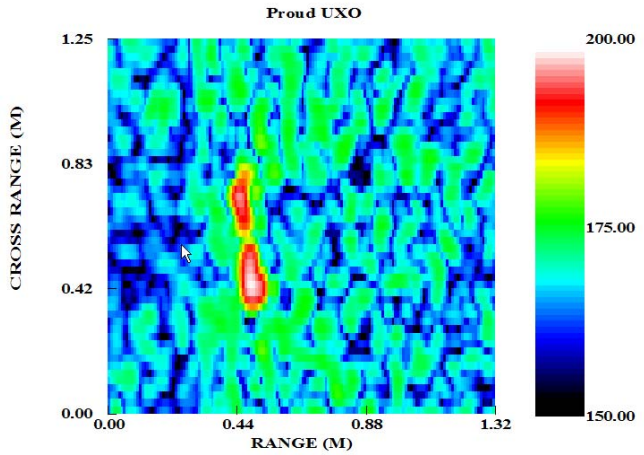

Figure 7. Blown up image of simulated mortar shell.

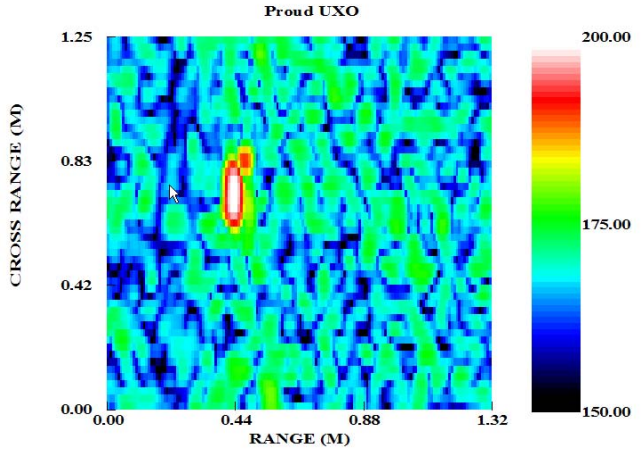

Figure 8. Blown up image of simulate 100 mm artillery shell.

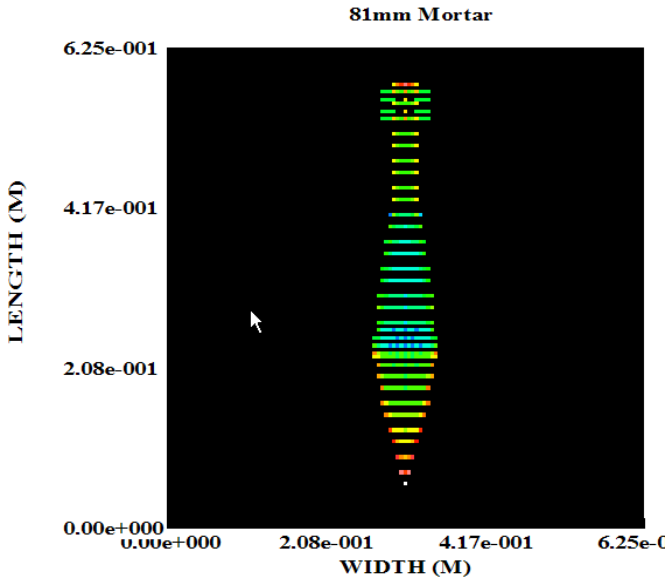

Figure 9. Outline of shape of 81 mm mortar shell.

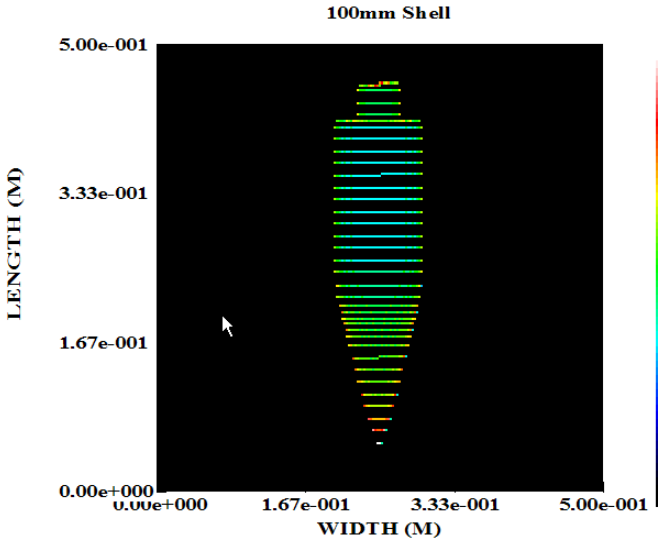

Figure 10. Outline of 100 mm artillery shell.

Figure 11 depicts an image of the same mortar shell, spherical shell, and 100mm artillery shell buried approximately 10cm. Near the sphere there is a partial image of a buried bomb case. Figure 12 depicts a blown up image of a simulated image of the mortar shell buried 10 cm. The measured and simulated images of the mortar shell are very similar in appearance. Figure 13 depicts a simulated image of the buried 100 mm shell. Note, the outline of the shape of the target.

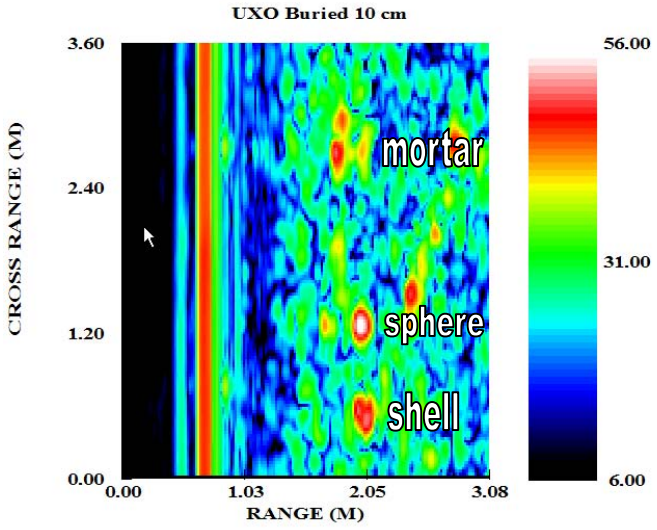

Figure 11. Image of UXO buried 10 cm.

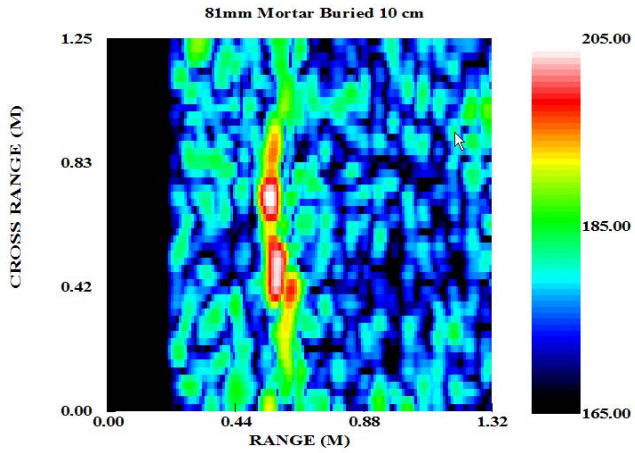

Figure 12. Simulated image of mortar shell buried 10 cm.

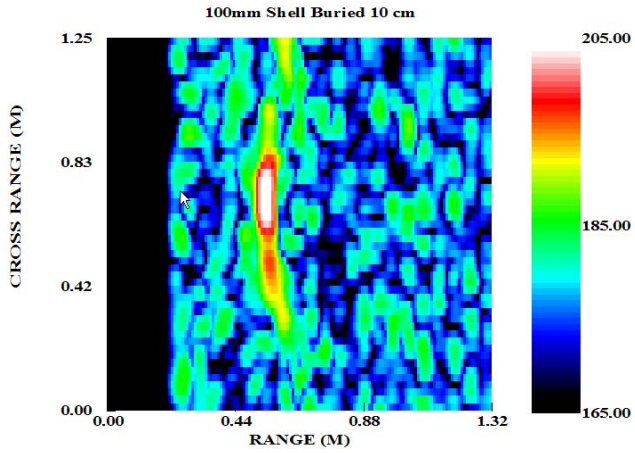

Figure 13. Simulated image of buried 100 mm shell.

V SUMMARY

Bragg diffraction of sound into the sediment is the dominant mechanism for sound penetrating the interface at sub-critical grazing angles. However, first and second order perturbation theory are inadequate to reproduce the measured signal-to-noise levels observed in the SAX99 experiment. Higher order terms are needed to account for Bragg scattering in the near vertical directions.

A better alternative than using higher order perturbation theory is to use the small slope approximation to describe sediment penetration from the ripple field. In the small wave height limit, the small slope approximation reduces to perturbation theory. However, the first order small slope approximation[6] is proportional to the Kirchhoff approximation, which includes all orders of Bragg scattering.

ACKNOWLEDGEMENTS

This work was jointly sponsored by SERDP (Strategic Environmental Research and Development Program) and code 32MIW of the Office of Naval Research.

REFERENCES

1) Moe, J.E., (1996), “Near and far-field acoustic scattering through and from 2-dimensional fluid-fluid rough interfaces”, Applied Physics Laboratory at the University of Washington, Technical Report 9606.
2) Sammelmann, Gary Steven, (2001), “Propagation and Scattering in Very Shallow Water”, Oceans 2001 conference proceedings.
3) Lim, Raymond, Kevin Williams, and Eric Thorsis, (2000), “Acoustic scattering by a three-dimensional elastic object near a rough surface”, Journal of the Acoustical Society of America, 107(3), pp. 1246-1262.
4) Jackson, Darrell, and Dale Winebrenner, (1988), “Comparison of perturbation theories for rough surface scattering”, Journal of Acoustical Society of America, 83(3), pp. 961-969.
5) Thorsis, Eric, Kevin Williams, Nicholas Chotiros, James Christoff, Kerry Commander, Charles Greenlas, Vance Holliday, Darrell Jackson, Joseph Lopes, Duncan McGehee, John Piper, Michael Richardson, and Dajun Tang, (2001), “An overview of SAX99: Acoustic measurements”, IEEE J. Oceanic Engineering 26(1), pp. 4-24.
6) Thorsis, Eric, and Shira Lynn Broschat, (1995), “An investigation of the small slope approximation for scattering from rough surfaces. Part I. Theory”, Journal of the Acoustical Society of America 97(4), pp. 2082-2093.